Centromere tethering confines chromosome domains

Jolien Suzanne Verdaasdonk[1], **Paula Andrea Vasquez**[2], **Raymond Mario Barry**[1], **Timothy Barry**[1], **Scott Goodwin**[1], **M. Gregory Forest**[3], and **Kerry Bloom**[1]

[1]Department of Biology, The University of North Carolina at Chapel Hill, Chapel Hill, NC 27599, USA

[2]Department of Mathematics, The University of South Carolina, Columbia, SC 29208, USA

[3]Department of Mathematics and Biomedical Engineering, The University of North Carolina at Chapel Hill, Chapel Hill, NC 27599, USA

Summary

The organization of chromosomes into territories plays an important role in a wide range of cellular processes including gene expression, transcription, and DNA repair. Current understanding has largely excluded the spatio-temporal dynamic fluctuations of the chromatin polymer. We combine *in vivo* chromatin motion analysis with mathematical modeling to elucidate the physical properties that underlie the formation and fluctuations of territories. Chromosome motion varies in predicted ways along the length of the chromosome, dependent on tethering at the centromere. Detachment of a tether upon inactivation of the centromere results in increased spatial mobility. A confined bead-spring chain tethered at both ends provides a mechanism to generate observed variations in local mobility as a function of distance from the tether. These predictions are realized in experimentally determined higher effective spring constants closer to the centromere. The dynamic fluctuations and territorial organization of chromosomes are, in part, dictated by tethering at the centromere.

Introduction

The foundations for our understanding of the physical organization of chromosomes originated in the work of Rabl and Boveri who articulated a characteristic conformation in which centromeres and telomeres are located at opposite sides of the nucleus and this organization is maintained throughout the cell cycle (Boveri, 1909; Cremer and Cremer, 2010; Rabl, 1885; Spector, 2003). Chromosomes in budding yeast display a Rabl-like configuration in interphase (reviewed in (Albert et al., 2012; Taddei and Gasser, 2012; Taddei et al., 2010; Zimmer and Fabre, 2011)). Centromeres are clustered and attached by microtubules to an unduplicated spindle pole body (SPB) (Dekker et al., 2002; Jin et al., 2000; O'Toole et al., 1999). Telomeres are located at the nuclear periphery in five to eight clusters in a manner dictated, at least in part, by chromosome arm length with telomeres on arms of similar lengths clustering together (Bystricky et al., 2005; Dekker et al., 2002;

Publisher's Disclaimer: This is a PDF file of an unedited manuscript that has been accepted for publication. As a service to our customers we are providing this early version of the manuscript. The manuscript will undergo copyediting, typesetting, and review of the resulting proof before it is published in its final citable form. Please note that during the production process errors may be discovered which could affect the content, and all legal disclaimers that apply to the journal pertain.

Supplemental Information
Supplemental Information includes Supplemental Experimental Procedures, five figures and two tables.

Hediger et al., 2002; Jin et al., 2000; Schober et al., 2008). More recently, the characterization of the physical organization of chromatin within the nucleus has been described using 3C (chromosome conformation capture) and high-throughput variants of this technique (de Wit and de Laat, 2012; Dekker et al., 2002; Dixon et al., 2012; Sanyal et al., 2011). Using a 4C (circular chromosome conformation capture) followed by deep sequencing protocol, Duan *et al* (Duan et al., 2010) showed that budding yeast chromosomes occupy discrete areas of the nucleus around the tethered centromeres. Population imaging of yeast nuclei has furthermore established the existence of chromosome territories (Berger et al., 2008) that are now perceived as a fundamental organizational feature of the nucleus (Austin and Bellini, 2010; Bickmore and van Steensel, 2013; Cremer and Cremer, 2010; Dixon et al., 2012; Hubner and Spector, 2010; Spector, 2003).

Various computational models have examined the formation of chromosomal territories and have shown that this organization can be explained by the inherent properties of a fluctuating polymer (Rosa and Everaers, 2008; Tjong et al., 2012; Wong et al., 2012). These models identify tethering, by simulating attachment at the centromere and telomere, and confinement, either by nuclear membrane or crowded polymer effects, as essential in modeling chromosome behavior and validate the starting point of our polymer model. By simulating the positioning of self-avoiding polymers, it has been suggested that entropic forces are sufficient to recapitulate the observed chromosomal territories (Cook and Marenduzzo, 2009; Finan et al., 2011). However, both the 3C variants and imaging to date have primarily examined the organization of nuclei in a whole population and lack information about the dynamics of chromatin organization within the cell nucleus.

We have quantified dynamic fluctuations along the length of the chromosome. The radius of confinement (R_c) is smaller at positions closer to the site of centromere attachment. We have examined the position dependent fluctuations using a bead-spring polymer model of chromatin together with the biological constraints of nuclear confinement, crowding, and tethering. *In vivo* chromatin tethering and fluctuations underlie chromosome organization and dynamics. Thus, the organization of chromatin within the nucleus of interphase yeast cells is dictated by its confinement and proximity to an attachment point and the dynamics can be approximated by the motion of an entropic spring.

Results

Chromatin confinement varies along the length of the chromosome

We examined the *in vivo* dynamics of chromatin during interphase to determine the wild type (WT) radius of confinement (R_c) at a discrete number of sites along the length of the chromosome. To do this, we tracked both a GFP-labeled chromatin array (lacO/lacI-GFP) at 6.8 kb (ChrXV), 8.8 kb (ChrIII), 24 kb (ChrIII), and 240 kb (ChrII) from the centromere (CEN) and relative to the unduplicated SPB (Spc29-RFP) over 10 minutes at 30 second intervals and measured sub-pixel localization by Gaussian fitting over time. The 240 kb lacO array is positioned roughly midway between the centromere and telomere. The distribution of spot positions show that arrays integrated further from the centromere can explore a larger space as compared to those more proximal to the point of attachment (Figure 1A). In order to quantify the sub-nuclear confinement observed, we use two methods to calculate R_c. From the plateau of the mean square displacement (MSD) curve (Figure 1B), 2D MSD gives (Neumann et al., 2012) (Experimental Procedures)

$$R_c = \frac{5}{4} * \sqrt{MSD_{plateau}}. \quad (1)$$

From the standard deviation of spot positions, σ, and the average squared deviation from the mean position, $\left\langle \Delta r_0^2 \right\rangle$, we applied the equipartition theorem to calculate R_c from random chromatin motion (Scheffold et al., 2010; Uhlenbeck and Ornstein, 1930) (Experimental Procedures),

$$R_c = \frac{5}{4} * \sqrt{2\sigma^2 + \left\langle \Delta r_0^2 \right\rangle}. \quad (2)$$

Equations 1 and 2 are not statistically different for positions close to the tether (Student's t-test, $p < 0.05$, Table S1, Figure S1A). The plateau value from MSD is more variable as it is based on long lag times between spot measurements and uses a fraction of the total data. Therefore, we use Equation 2 and the standard deviation obtained with the entire data set to calculate R_c throughout this work.

The R_c is largest for the chromatin spot furthest from the centromere at 240 kb (705 nm, 43 cells) and smallest for spots proximal to the centromere at 8.8 kb (274 nm, 40 cells) and 6.8 kb (396 nm, 54 cells), suggesting that the attachment at the centromere functions to constrain chromatin movement (Figure 1C, Table 1). Statistical comparison revealed that R_c values of chromatin spots at these four distances from the centromere are all statistically different from each other (Levene's test, $p < 0.05$, Figure S2A) (Levene, 1960). This pattern is a generalized feature of chromosomes in yeast (Figure 1D) (Bystricky et al., 2005; Dion et al., 2012; Hediger et al., 2002; Heun et al., 2001; Mine-Hattab and Rothstein, 2012; Neumann et al., 2012).

Chromatin dynamics in interphase are dictated by tethering

In order to determine whether the R_c observed adjacent to the centromere is dictated by microtubule attachment or an inherent property of the pericentric chromatin, we tracked chromatin motion in cells in which the centromere has been detached through its conditional inactivation (Hill and Bloom, 1987) (Figure 2A). The insertion of the GAL promoter adjacent to the centromere allows the centromere to function normally when grown on glucose and inactivated when on galactose. Detachment upon centromere inactivation results in a dramatic increase in the R_c at 8.8 kb from the CEN from 274 nm (40 cells) to 745 nm (23 cells) (Figure 2B, Table 1), demonstrating that this chromatin region can explore a larger space when no longer attached to the SPB. This increased motion is unlikely the result of transcription induced by the GAL promoter as these loci have previously been shown to be confined at the periphery (Brickner et al., 2007; Drubin et al., 2006). Chromatin confinement at maximal distance from attachment (lacO at 240 kb) and detached upon centromere inactivation (Gal-CEN at 8.8 kb on galactose) is not statistically different (Levene's test, $p < 0.05$). LacO at 8.8 kb is statistically different from both lacO at 240 kb and Gal-CEN at 8.8 kb (Levene's test, $p < 0.05$, Figure S2A). This indicates that the confinement of the 8.8 kb chromatin spot is due to attachment at the centromere and not an inherent property of this region of chromatin. The tethering of chromatin is a universal organizational feature and has important implications for the temporal and spatial fluctuations of chromosomes.

The chromatin polymer behaves like an elastic filament during interphase

Throughout our *in vivo* time lapse movies, we observed transient spot expansion of lacO/lacI-GFP labeled chromatin arrays in G1 (Figure 3A-D). Chromatin arrays stretch during mitosis, presumably as a consequence of microtubule pulling force (Stephens et al., 2011; Stephens et al., 2013). Spot expansion during G1 could be the result of microtubule dynamics (as chromosomes remain attached at their centromeres) and/or the inherent spring properties of the polymer. We defined a change in the lacO arrays by measuring the ratio of

the axes of a 2D Gaussian fit to the GFP signal. A spot was defined as expanded when the long axis was at least 1.5 times larger than the smaller axis. The lacO/lacI-GFP array at 240 kb from the CEN was found to exhibit expansion in 16% of time points imaged (141/879 planes) and the centromere-proximal (6.8 kb from the CEN) chromatin spot exhibited expansion in 10% of time points imaged (109/1105 planes) (Figure 3A and C). Examples of lacO/lacI-GFP dynamics in live cells are plotted in Figure 3B (240 kb) and D (6.8 kb). These transient extensions are of relatively short duration, lasting less than a few minutes. On average, the chromatin spot at 240 kb from the CEN had higher mean and median ratios than the 6.8 kb chromatin spot (Figure S3A). We observe recoiling of these chromatin spots, indicating that the chromatin is behaving like an elastic filament. The spot expansion and contraction is variable and often deformed (see variability of expansion shapes, Figure 3A and C), thus chromatin motion in interphase shows no coherent properties. The random trajectory of energy-dependent processes acting on the chromatin validates the rationale for using the equipartition theorem to estimate confinement (Equation 2). In addition to aspect ratio, we examined variance in distance between two loci (lacO/lacI-GFP and tetO/tetR-CFP) adjacent to the centromere of chromosome XI to assess chromatin polymer elasticity (Figure S3B). We find that both aspect ratio and variance in spot distances reveal the elastic nature of the chromatin.

Modeling the chromatin spring as a doubly tethered, confined bead-spring chain with excluded volume interactions can recapitulate experimental dynamics

In order to model the dynamic behavior and gain insight into chromosome organization, we construct a 2D bead-spring model of a doubly tethered polymer chain, using Brownian beads connected by linear springs (Doi and Edwards, 1986) (Experimental Procedures, Figure 4A). The chain is tethered at both ends to simulate the centromere and telomere attachments, confined within a 1 μm circle (the nucleus), and subject to excluded volume interactions. The bead-spring chain has a persistence length (L_p) of 50 nm, corresponding to the known value for DNA. The L_p is defined as the distance over which the correlation of the direction of the two ends is lost, and longer L_p implies stiffer polymer chains (Bloom, 2008). We model one arm of a chromosome as 100 beads connected by 99 springs with a packing density in between that of the 11 nm and 30 nm fibers (Experimental Procedures, "Defining model variables"). R_c values along the chain compare to experimental values and are smaller at positions closer to the tether point (Figure 1C, black squares). The varying radii of confinement observed *in vivo* can be recapitulated by a doubly tethered bead-spring model. We note that in the absence of tethering, all positions within the chain will have the same R_c (i.e., the radius of the circle) (Rosa and Everaers, 2008). Thus tethering results in variations of R_c with respect to the distance from the centromere. We found that the *qualitative* behavior of R_c along the chain remains unchanged when the radius of the nucleus is changed, however the magnitude of R_c decreases with the radius.

While the bead-spring chain consists of identical springs between each pair of beads, the effects of tethering, geometric confinement, and excluded volume interactions result in distinct statistical fluctuations of each bead (lacO/lacI-GFP position experimentally) along the chain. This leads to a *position-dependent effective spring constant* (k_s), as seen by a particular bead relative to the tether points, and measured based on that bead's fluctuations as described below. The tendency of the spring to adopt a random coil can be represented in terms of a spring constant that reflects the spring stiffness (Bloom, 2008). The effective spring constant (k_s) for bead in our model is given by

$$k_{s,i} = 3k_B T \left(\frac{c_r}{2 L_p x L_c} \right) \left(\frac{1}{p(1-p)} \right). \quad (3)$$

where k_B is the Boltzmann constant, T is temperature (Kelvin), L_p is persistence length, L_c is contour length, C_r is ratio of compaction, and p is the percentage of the chain from the centromere (Experimental Procedures). From the displacement of the beads in our model, we estimate k_s as a function of position along the chain (Figure 4B). This observation reveals the limitation in deducing a spring constant from measurements of a single spot along the chain. The k_s is smaller for beads that "explore" a larger space, and so the k_s will be highest (most stiff) for positions close to the tether point and softest in the middle of the chain. Thus, tethering of an otherwise homogeneous bead-spring chain results in a gradient of k_s along the chain and introduces variations in local mobility.

The effective spring constant along the entropic chromatin spring can be measured in vivo

We calculate an effective k_s from our *in vivo* time lapse data using two methods (Experimental Procedures). Using the MSD plateau value and the average squared deviation of each step from the mean position $\left\langle \Delta r_0^2 \right\rangle$, we calculated (Bruno et al., 2011; Kamiti and van de Ven, 1996),

$$k_s = \frac{2k_B T}{\langle MSD_{plateau} \rangle - \langle \Delta r_0{}^2 \rangle}. \quad (4)$$

Using the equipartition theorem, we measured the standard deviation (σ) of each step from the mean position to calculate (Scheffold et al., 2010),

$$k_s = \frac{k_B T}{\sigma^2}. \quad (5)$$

Similar to R_c, k_s values were calculated using both methods for lacO at 6.8 kb, 8.8 kb, 24 kb, and 240 kb from the CEN (Figure S1B, Table S1). We found significant agreement between the two methods; a Student's t-test comparing k_s values calculated using Equations 4 and 5 for individual cells showed no statistical differences between the two methods (Student's t-test, $p<0.05$). As previously described for R_c calculations, the plateau method uses a fraction of the total data set. Thus we use the equipartition method (Equation 5) and the standard deviation obtained from the entire data set for remaining calculations.

From Equation 5, we see that in general stiffness varies inversely with position variance, meaning that for loci exhibiting smaller variance, the chromatin will have a higher effective spring constant (Figure 1A). As predicted by our model, k_s was found to vary with distance from the tether point, and appeared stiffer at points closer to the site of attachment and regions within the pericentromere domain exhibit a variation in stiffness (lacO at 6.8 kb- 1.6×10^{-4} pN/nm; 8.8 kb- 3.4×10^{-4} pN/nm; 24 kb- 1.3×10^{-4} pN/nm; 240 kb- 5.1×10^{-5} pN/nm) (Figure 4D, Table 1). Statistical comparison of population variances showed these to all be significantly different from each other (Levene's test, $p<0.05$, Figure S2A). Application of equipartition methods to our data represents a starting point to quantify these dynamics, and further work will refine the applied mathematics to more closely match *in vivo* conditions.

Upon detachment from the centromere (Gal-CEN), the k_s for a chromatin spot 8.8 kb from the CEN is reduced as compared to WT at 8.8 kb and appears softer and approaches the value of the chromatin arm at 240 kb (Gal-CEN at 8.8 kb- 4.6×10^{-5} pN/nm, Figure 4D, Table 1). Statistical comparison found Gal-CEN at 8.8 kb to be significantly different from WT at 8.8 kb but not significantly different from WT at 240 kb (Levene's test, $p<0.05$, Figure S2A). This confirms the prediction that the apparent properties of the chromatin polymer are dictated by the attachment to a tether point like the centromere. The gradient of

k_s is the result of tethering and provides a mechanism to build variations in local mobility along the chromatin chain. This implies a role for tethering in the differential regulation of various regions of chromatin by altering polymer properties such as dynamics and stiffness. By attaching or detaching chromatin from a tether, the cell can efficiently alter the stiffness, as well as the range of motion of the chromatin.

Cohesin contributes to local clamping of chromatin

A major source of chromatin organization is the structural maintenance of chromosomes (SMC) protein complex cohesin. While the role of cohesin in holding sister chromatids together in mitosis is well-established, it is becoming increasingly evident that cohesin also serves a vital role in interphase chromatin gene regulation through looping (as reviewed in (Haering and Jessberger, 2012; Seitan and Merkenschlager, 2012; Sofueva and Hadjur, 2012)). Given the regulatory role for cohesin looping, we predict a role for cohesin in the organization of chromatin into territories and maintaining chromatin dynamics during interphase.

We examined R_c and effective k_s of the lacO/lacI-GFP array at 240 kb from the CEN in WT and *mcd1-1* cells at permissive (24°C) and restrictive (37°C) temperature (Figure 5A). The R_c is increased in *mcd1-1* cells at restrictive temperature as compared to *mcd1-1* at permissive or WT (WT at 24°C- 705 nm, 43 cells; WT at 37°C- 691 nm, 16 cells; *mcd1-1* at 24°C- 892 nm, 25 cells; *mcd1-1* at 37°C- 958 nm, 33 cells; Figure 5B, Table 1). This does not result from increased temperature, as WT cells at 37°C do not show a similar increase in R_c. In addition, k_s is decreased in *mcd1-1* cells at restrictive temperature as compared to WT at 37°C, suggesting that the chromatin spring is softer upon the loss of cohesin (WT at 24°C- 5.1×10^{-5} pN/nm; WT at 37°C- 5.4×10^{-5} pN/ nm; *mcd1-1* at 24°C- 3.2×10^{-5} pN/ nm; *mcd1-1* at 37°C- 2.8×10^{-5} pN/ nm; Figure 5C, Table 1). Statistical comparison of population variances found no statistical difference between WT at 24°C and WT at 37°C, whereas *mcd1-1* at 24°C and *mcd1-1* at 37°C were both statistically different from WT and from each other (Levene's test, p<0.05, Figure S2B).

To model the reduction of cohesin and predict its physiological role, we have examined the dynamics of chains composed of more beads (from N=100 to N=150 at a constant $L_p = 50$ nm) (Experimental Procedures, Figure 5D). We reason that chromatin in loops will not contribute to the effective chromatin length, and upon loss of cohesin and release of loops, additional chromatin will lengthen the chain. In the model this reduces the compaction ratio, and at the same L_p, which increases the number of beads (# of beads = $(L_c/C_r)/2L_p$)). The model predicts that upon an increase in effective chromatin length (i.e., more beads in the chain), the R_c for any given point should increase and the k_s will decrease (Figure 5D), consistent with the experimental results.

Nucleosome depletion results in a stiffer chromatin fiber

We hypothesize that changes to nucleosome density would have important effects on chromatin fluctuations. We tested the effects of changing chromatin packaging on dynamics by measuring R_c and effective k_s in cells with reduced nucleosome occupancy. We measured the MSD dynamics of a chromatin spot 6.8 kb from the CEN in a stain depleted of histone H3 that results in a 2-fold reduction of nucleosome density (Bouck and Bloom, 2007) (Figure 5E). The R_c was statistically significantly reduced from 396 nm (54 cells) to 319 nm (55 cells) (Levene's test, p<0.05, Figure 5F, Table 1, Figure S2C). The k_s was statistically significantly increased, becoming slightly stiffer from 1.6×10^{-4} pN/nm to 2.5×10^{-4} pN/nm (Levene's test, p<0.05, Figure 5G, Table 1). These effects were not due to α factor arrest, which was not found to significantly alter R_c or k_s (Figures 5E-G, Table 1, Figure S2C). From these data, we conclude that nucleosomal packaging is an important

factor in dictating the spatio-temporal organization and fluctuations of the chromatin polymer.

The reduced nucleosomal density in H3 depleted cells will increase the fraction of naked DNA from ~20 bp/nucleosome (based on linker length) to ~160 bp/2 nucleosomes, or ~80 bp/nucleosome (based on loss of ½ the number of nucleosomes). This will disproportionally alter the physical properties of the chromatin. Unlike cohesin depletion in which the fraction of naked DNA is constant, we model the increase in naked DNA as a decrease in persistence length (L_p). Bystricky et al. have reported that DNA has a substantially shorter L_p than chromatin (Bystricky et al., 2004). The model predicts that by decreasing L_p, R_c for any given bead decreases (data not shown) and its k_s increases (Figure 5H).

The lacO/lacI-GFP spot morphology provides a quantitative assay for chromatin elasticity. The centromere-proximal (6.8 kb) chromatin spot exhibited expansion in 10% of time points imaged (WT, 109/1105 time points) and reduced to 3% upon histone H3 depletion (36/1148 time points) (Figure 3E). The stiffer k_s at 6.8 kb from the CEN observed in nucleosome depleted cells would predict that fewer cells would exhibit expansion (aspect ratio > 1.5) of the centromere-proximal lacO/lacI-GFP array since it would take more energy to extend the entropic spring. Reduced nucleosome density would result in unwrapping of the DNA from nucleosomes and a general increase in spot size. We examined the morphology of the centromere-proximal lacO/lacI-GFP labeled chromatin spot and observed an average increase in spot size for both compacted (aspect ratio < 1.5) and decompacted (aspect ratio >1.5) spots (Figure S4). We have directly assessed the dynamic physical consequences of changing the histone compaction and measured a higher effective k_s for a chromatin spot 6.8 kb from the CEN in nucleosome depleted cells. Nucleosomal density and therefore L_p and linker length are important factors in determining the physical properties of the entopic chromatin spring.

Dynamic fluctuations underlie chromosome territories

Chromosome territories within a population of cells can be visualized in chromosome interaction maps. In order to examine if our tethered bead-spring model describes the formation of chromosome territories within the dynamic nucleus, we generate interaction maps of four tethered chains within a circle. We examined the bead position distributions in our polymer model (Figures 7A-B) and plotted the average normalized bead separation (Figures 7C-D). Telomeric attachment in budding yeast is known to occur in five to eight foci and in Rabl-like configuration (Bystricky et al., 2005), and therefore we consider either five attachment points analogous to one centromere position and four discrete telomere attachment points (Figure 7A), or three attachment points (one centromere position and two telomere points) (Figure 7B). The combination of excluded volume interactions and shorter distance between tether points results in a more uniform heat map distribution (Figures 7A and C - chains 1 and 4, Figures 7B and D - chains 3 and 4). When the tethers are further apart and the chain is able to explore a larger space, beads along the middle of the chain rarely come into contact (blue on the heat maps) and excluded volume interactions dominate over confinement. The chromosome interaction maps reveal a potential regulatory mechanism in the position of the telomere attachment site. The tethered regions of a single chain, while sampled infrequently, provide the ability for disparate chains to physically interact with one another. This provides a mechanism for distinct chains within the nucleus to share genetic information, while satisfying the territories of individual chains.

Discussion

In vivo measurements of fundamental chromosome properties – R_c and effective k_s

Through a combination of experimental observation and mathematical modeling we have shown that interphase chromatin fluctuations are mainly governed by attachment at the centromere and telomere. Loss of attachment allowed centromere-proximal chromatin to soften (lower effective k_s) and explore more space (higher R_c), behaving like a region out on the chromosome arm. By formulating a 2D bead-spring model based on simple polymer physics, we capture the observed k_s along the length of the chromosome. To capture relevant experimental features the model requires: (1) tethering at both ends, (2) confinement within a domain, and (3) excluded volume interactions between beads.

In order to determine the effect of polymer length on chromosome fluctuations, we examined dynamics in cohesin-depleted cells. Loss of cohesin effectively lengthens the chromosome since less of the total length is confined in loops. This led to softening of the chromatin fiber at 240 kb from the CEN and allowed this region to explore a larger space. Thus, the overall length of the chromosome is an important factor in determining its spatio-temporal fluctuations, consistent with polymer theory (Equation 6) in which the spring constant is inversely related to number of segments (N). In addition to chromosome length, the persistence length (L_p) of the polymer is predicted to play an important role in chromosome fluctuations. As L_p is decreased, the spring constant will increase by virtue of the increase in number of entropic states, and the polymer will occupy a smaller radius of gyration (Bloom, 2008). In order to test this, we hypothesized that reduced nucleosome occupancy results in a lower average persistence length (DNA L_p = 50 nm vs. chromatin L_p = 170-220 nm (Bystricky et al., 2004)). Consistent with the theory, we observed stiffening of the centromere-proximal chromatin (higher k_s) and smaller R_c in nucleosome depleted cells.

Examining chromosome territories to understand cellular behaviors like repair

Our *in vivo* observations of chromatin fluctuations highlight dynamics and predict significant interactions to allow for a variety of cellular processes (Figure 7). We hypothesize that the organization of chromosomes within the nucleus into territories dictates chromosome interactions. Altering the location of tethering or detaching one chromosome end would allow chromatin to explore a larger volume. These genome-wide changes could be quickly reversed by subsequent reattachment of the chromosomes. The radius of confinement is determined by multiple factors including tethering, compaction by cohesin, and nucleosomal wrapping (Figures 1D, 2B, 5B and 6B). Various model systems have shown that the total radius of confinement is similar across species (Chubb and Bickmore, 2003; Gasser, 2002; Soutoglou and Misteli, 2007), suggesting that this may be at least in part dictated by an inherent property of the polymer. Attenuation of these properties could contribute to facilitating chromosome interactions upon damage, and form the basis for mechanism of action for a wide range of pathways that serve to increase or decrease chromatin motion such as DNA repair or gene gating. Based on the increased confinement and stiffening of the chromosome upon reduction of nucleosome occupancy, we hypothesize that attenuation of nucleosomal wrapping could play an important role in dictating the dynamics of DNA repair by reducing persistence length. We have previously shown that dynamic exchange of nucleosomes is important for maintenance of the pericentromeric chromatin under tension (Verdaasdonk et al., 2012). The work presented here provides a basic framework for an integrated understanding of physical organization and dynamic interactions dictated by chromatin modifications to explain complex cellular behaviors such as DNA repair.

Changes in the radius of confinement have been observed upon DNA damage, both for damaged and undamaged chromosomes (Dion et al., 2012; Haber and Leung, 1996; Mine-Hattab and Rothstein, 2012). The increased range of motion of a DSB is thought to allow the damaged site to explore a much larger area within the nucleus to promote homology search for repair. The increased motion of damaged chromatin is known to require the recombination proteins Rad51 and Rad54, and the DNA damage response pathway components Mec1 and Rad9 (Dion et al., 2012; Mine-Hattab and Rothstein, 2012). Interestingly, Mec1 checkpoint activity is important to maintain replication fork integrity by detaching tethered and highly transcribed regions from the nuclear pore (Bermejo et al., 2011). This mechanism of detachment cannot explain the increased motion observed upon DNA damage (Ira and Hastings, 2012), but could suggest an alternative role for the DNA damage response pathway in maintaining chromatin tethering. These data highlight the importance of tethering to regulate chromatin motion, and further work should examine which points of tethering are altered upon DNA damage.

Experimental Procedures

For detailed growth and imaging conditions, see supplemental experimental procedures. Strains used are listed in Table S2.

Image analysis

For MSD analysis, the images were identically analyzed using MetaMorph (Molecular Devices, Sunnyvale, CA, USA) and MATLAB (The Mathworks, Natick, MA, USA). The GFP and RFP foci of the brightest planes per time point were tracked using a custom MATLAB program (Speckle Tracker) as previously described (Wan, 2008; Wan et al., 2012; Wan et al., 2009). These coordinates were further analyzed using MATLAB and Excel (Microsoft, Redmond, WA, USA) software to determine mean square displacement. The RFP coordinates were subtracted from the GFP coordinates to eliminate cell and nuclear motion. We then examined the 2D change in position of the lacO/lacI-GFP chromatin spot over increasing time lags using a classical MSD approach at each time interval,

$$MSD_\tau = \left\langle (x_{t+\tau} - x_t)^2 + (y_{t+\tau} - y_t)^2 \right\rangle, \quad (6)$$

for all time lags τ. Only cells whose MSD curves exhibited a linear slope within the (1.5*IQR) range were included in subsequent analysis. Figures were made using SigmaPlot (Systat Software, San Jose, CA, USA).

To measure spot size, we used a custom GUI written in MATLAB as described previously (Haase et al., 2012). The spot intensity distribution is fit with a two-dimensional Gaussian function and full width-full maximum values are used to determine spot size.

Calculating R_c from experimental data

We calculate R_c from the 2D MSD plateau value as (Neumann et al., 2012)

$$R_c = \frac{5}{4} * \sqrt{MSD_{plateau}}. \quad (1)$$

where the plateau is measured from the 330 – 390 s region of the timelapse, as most cells have reached confinement at this point while minimizing potential errors introduced by MSD analysis at longer time lags.

We calculate the variance of the distribution of spot positions as $\sigma^2 = mean\left(\sigma_x^2, \sigma_y^2\right)$ where these are measured using MATLAB to fit the spot positions as $[\mu_x, \sigma_x] = normfit(x - x_{mean})$ and $[\mu_y, \sigma_y] = normfit(y - y_{mean})$. We then use σ^2 to calculate R_c as

$$R_c = \frac{5}{4} * \sqrt{2\sigma^2 + \langle \Delta r_0^2 \rangle}, \quad (2)$$

where the average squared deviation from the mean position is $\langle \Delta r_0^2 \rangle = \langle \Delta x_0^2 \rangle + \langle \Delta y_0^2 \rangle$.

Entropic Bead-Spring Chain Model

We model chromosomes as chains composed of N+1 beads connected by N linear springs. The equation of motion for a bead i at position X_i is given by (Doi and Edwards, 1986),

$$\frac{x\widehat{X}_i}{d\hat{t}} = \frac{1}{\zeta}\left(\widehat{F}_i^B(t) + \widehat{F}_i^S(t) + \widehat{F}_i^{EV}(t) + \widehat{F}_i^W(t)\right), \quad (7)$$

for $i = 0, 1, \ldots, N + 1$. Here ζ is the bead drag coefficient, F_i^B is the Brownian force, F_i^S is the spring force, F_i^{EV} is the excluded volume force, and F_i^W captures the interaction of the bead with the cell walls. In this work we use the following dimensionless variables,

$$X_i = \widehat{X}_i \sqrt{\frac{k_s^0}{k_B T}}, \quad t = \hat{t}\frac{2k_s^0}{\zeta}, \quad F = \widehat{F}\frac{1}{\sqrt{k_s^0 k_B T}}, \quad \text{where} \quad k_s^0 = \frac{3\,k_B T}{(2L_p)^2}. \quad (8)$$

- *Brownian force.* The Brownian force is $\widehat{F}_i^B = \sqrt{2k_B T \zeta}W_i$, or in dimensionless form,

$$F_i^B = W_i, \quad (9)$$

  where W_i is a Wiener process:

$$\begin{aligned}\langle W_i(t) \rangle &= 0, \\ \langle W_i(t)\,W_j(t') \rangle &= \delta_{ij}\,\min\left(t, t'\right).\end{aligned}$$

- *Spring force.* We consider linear springs so that the spring force acting on bead i is,

$$F_i^S = 2X_i - X_{i-1} - X_{i+1}, \quad (10)$$

  for $i = 1, 2, \ldots, N$.

- *Excluded volume force.* The excluded volume interaction is modeled using a soft potential as in (Jendrejack, 2002),

$$F_i^{EV} = \frac{Z}{4d^5}\left(\sum_{j=0, j\neq i}^{N}(X_i - X_j)\exp\left[-\frac{(X_i - X_j)^2}{2d^2}\right]\right), \quad (11)$$

  here the dimensionless parameters z and d are, respectively, measures of the strength and range of the interaction.

- *Wall interaction*. To model the bead-wall interaction, whenever a bead moves outside the confining circle, it is moved to the nearest point on the boundary before the next time step (Jones et al., 2011).

Effective spring constant in a double-tethered Rouse chain

If consider that the only forces are $\boldsymbol{F}_i^B$ and $\boldsymbol{F}_i^S$ the model becomes a double-tethered Rouse chain. In this case the effective spring constant for bead *i* can be found explicitly as,

$$k_{s,i}=3k_B T \left(\frac{c_r}{2L_p \times L_c} \right) \left(\frac{1}{p(1-p)} \right), \quad (3)$$

where k_B is the Boltzmann constant, T is temperature (Kelvin), L_p is persistence length, L_c is contour length, C_r is ratio of compaction, and p is the percentage of the chain from the centromere (i.e., for centromere p=0 and for the telomere p=1). The first term, $3k_B T$, is the thermal contribution, the second, $\left(\frac{c_r}{2L_p \times L_c} \right)$, captures the properties of the chromatin, and the last, $\left(\frac{1}{p(1-p)} \right)$, measures relative location within the chromatin.

Defining model variables

The model requires two parameters: N and L_p. To determine N, we first estimate chromosome length in the cell by dividing the chromosome length in bp (contour length, L_c) by the packing density (ratio of compaction, C_r). For an average chromosome L_c ~800,000 bp and a packing density is 80 bp/nm (~4X nucleosomal chromatin), then its length in the nucleus is 10,000 nm (L_c/C_r). The packing density is less than the 30 nm fiber (~6X the 11 nm fiber) due to the lack of evidence for the 30 nm fiber and the reduced compaction of yeast chromatin relative to chromosomes in larger cells. The number of beads is derived from the nuclear length divided by the persistence length (L_p), 10,000 nm/50 nm = 200 beads. Since we model the polymer from the centromere to the telomere, we use N = 100 beads. L_p and packing density vary proportionally and cannot be independently deduced from the model. Simulations of 100 beads with L_p = 50 nm or 25 beads with L_p = 100 nm predict motion plots comparable to that shown in Figure 1A. The modeled R_c using 100 beads and L_p = 50 nm compares closely with literature values (dashed line, Figure 1D). These assigned values are not unique parameters, and it is likely that *in vivo* conditions include a wide range of values.

Calculating effective k_s from experimental data

Although the motion *in vivo* is ATP-dependent (Figure S5) (Weber et al., 2012), it is still random in nature with step sizes following a Gaussian distribution, supporting the assumption that the beads move in a harmonic potential well at some effective temperature (Tokuda et al., 2012). In this manner, it is possible to group the different components of energy-dependent motion in the single non-directional temperature parameter (T).

To calculate effective k_s from the plateau value of the 2D MSD plot, we consider the equation (Uhlenbeck and Ornstein, 1930)

$$MSD=2\frac{k_B T}{k_s} \left(1 - e^{-\zeta t/(2k_s)} \right) +2 \left\langle \Delta r_0^2 \right\rangle \left(1 - e^{-\zeta t/(k_s)} \right)^2. \quad (12)$$

This means that when *t* is very large, the plateau value is

$$MSD_{\text{plateau}} = 2\frac{k_{\text{B}}T}{k_{\text{s}}} + \left\langle \Delta r_0^2 \right\rangle, \quad (13)$$

where the average squared deviation from the mean position is

$$\left\langle \Delta r_0^2 \right\rangle = \left\langle \Delta x_0^2 \right\rangle + \left\langle \Delta y_0^2 \right\rangle. \quad (14)$$

Solving Equation 13 gives the spring constant as,

$$k_{\text{s}} = \frac{2k_{\text{B}}T}{MSD_{\text{plateau}} - \left\langle \Delta r_0^2 \right\rangle}. \quad (4)$$

To illustrate how to calculate effective k_{s} from variance of lacO spot position, we look at the simplest case: a bead moving by Brownian motion and attached to a fixed point by a linear spring. The bead position obeys the following Lagevin Equation,

$$\zeta d\mathbf{X} = -k_{\text{s}}\boldsymbol{X}dt + \sqrt{2k_{\text{B}}T\zeta}d\mathbf{W} \quad (15)$$

where, as before, $\mathbf{W}$ is a Wiener process.

Equation 15 has a corresponding Fokker-Planck Equation with solution,

$$P\left(\boldsymbol{X}\right) = \sim \exp\left(-\frac{k_{\text{s}}}{k_{\text{B}}T}\frac{\boldsymbol{X}^2}{2}\right). \quad (16)$$

This means that a histogram the distribution of bead positions has a Gaussian form with variance $\sigma^2 = k_BT/k_s$. Then from the variance of the distribution, one can obtain the spring constant as,

$$k_{\text{s}} = \frac{k_{\text{B}}T}{\sigma^2}. \quad (5)$$

Statistical analysis

We used the equipartition Equations 2 and 5 and the standard deviation from the whole population of cells for remaining comparisons. This results in a single value from the whole population standard deviation (with no associated error bars) and for statistical comparison we compare the homogeneity of population variances by Levene's test (Figure S2) (Levene, 1960). For additional details, see Supplemental Information and Figure S1.

Supplementary Material

Refer to Web version on PubMed Central for supplementary material.

Acknowledgments

Abbreviations used in this paper

SPB	spindle pole body
R_c	radius of confinement
WT	wild type
GFP	green fluorescent protein
RFP	red fluorescent protein
CEN	centromere
MSD	mean square displacement
GAL	galactose
k_s	spring constant
L_c	contour length
L_p	persistence length
C_r	compaction ratio

References

Albert B, Leger-Silvestre I, Normand C, Gadal O. Nuclear organization and chromatin dynamics in yeast: biophysical models or biologically driven interactions? Biochim Biophys Acta. 2012; 1819:468–481. [PubMed: 22245105]

Austin CM, Bellini M. The dynamic landscape of the cell nucleus. Mol Reprod Dev. 2010; 77:19–28. [PubMed: 19650114]

Berger AB, Cabal GG, Fabre E, Duong T, Buc H, Nehrbass U, Olivo-Marin JC, Gadal O, Zimmer C. High-resolution statistical mapping reveals gene territories in live yeast. Nat Methods. 2008; 5:1031–1037. [PubMed: 18978785]

Bermejo R, Capra T, Jossen R, Colosio A, Frattini C, Carotenuto W, Cocito A, Doksani Y, Klein H, Gomez-Gonzalez B, et al. The replication checkpoint protects fork stability by releasing transcribed genes from nuclear pores. Cell. 2011; 146:233–246. [PubMed: 21784245]

Bickmore WA, van Steensel B. Genome architecture: domain organization of interphase chromosomes. Cell. 2013; 152:1270–1284. [PubMed: 23498936]

Bloom KS. Beyond the code: the mechanical properties of DNA as they relate to mitosis. Chromosoma. 2008; 117:103–110. [PubMed: 18060422]

Bouck DC, Bloom K. Pericentric chromatin is an elastic component of the mitotic spindle. Curr Biol. 2007; 17:741–748. [PubMed: 17412588]

Boveri T. Die Blastomerenkerne von *Ascaris megalocephala* und die Theorie der Chromosomenindividualität. Arch Zellforsch. 1909; 3:181–268.

Brickner DG, Cajigas I, Fondufe-Mittendorf Y, Ahmed S, Lee PC, Widom J, Brickner JH. H2A.Z-mediated localization of genes at the nuclear periphery confers epigenetic memory of previous transcriptional state. PLoS Biol. 2007; 5:e81. [PubMed: 17373856]

Bruno L, Salierno M, Wetzler DE, Desposito MA, Levi V. Mechanical Properties of Organelles Driven by Microtubule-Dependent Molecular Motors in Living Cells. PLoS One. 2011; 6

Bystricky K, Heun P, Gehlen L, Langowski J, Gasser SM. Long-range compaction and flexibility of interphase chromatin in budding yeast analyzed by high-resolution imaging techniques. Proc Natl Acad Sci U S A. 2004; 101:16495–16500. [PubMed: 15545610]

Bystricky K, Laroche T, van Houwe G, Blaszczyk M, Gasser SM. Chromosome looping in yeast: telomere pairing and coordinated movement reflect anchoring efficiency and territorial organization. J Cell Biol. 2005; 168:375–387. [PubMed: 15684028]

Chubb JR, Bickmore WA. Considering nuclear compartmentalization in the light of nuclear dynamics. Cell. 2003; 112:403–406. [PubMed: 12600306]

Cook PR, Marenduzzo D. Entropic organization of interphase chromosomes. J Cell Biol. 2009; 186:825–834. [PubMed: 19752020]

Cremer T, Cremer M. Chromosome territories. Cold Spring Harb Perspect Biol. 2010; 2:a003889. [PubMed: 20300217]

de Wit E, de Laat W. A decade of 3C technologies: insights into nuclear organization. Genes Dev. 2012; 26:11–24. [PubMed: 22215806]

Dekker J, Rippe K, Dekker M, Kleckner N. Capturing chromosome conformation. Science. 2002; 295:1306–1311. [PubMed: 11847345]

Dion V, Kalck V, Horigome C, Towbin BD, Gasser SM. Increased mobility of double-strand breaks requires Mec1, Rad9 and the homologous recombination machinery. Nat Cell Biol. 2012; 14:502–509. [PubMed: 22484486]

Dixon JR, Selvaraj S, Yue F, Kim A, Li Y, Shen Y, Hu M, Liu JS, Ren B. Topological domains in mammalian genomes identified by analysis of chromatin interactions. Nature. 2012; 485:376–380. [PubMed: 22495300]

Doi, M.; Edwards, SF. The theory of polymer dynamics. Clarendon Press; Oxford University Press; Oxford: 1986.

Drubin DA, Garakani AM, Silver PA. Motion as a phenotype: the use of live-cell imaging and machine visual screening to characterize transcription-dependent chromosome dynamics. BMC Cell Biol. 2006; 7:19. [PubMed: 16635267]

Duan Z, Andronescu M, Schutz K, McIlwain S, Kim YJ, Lee C, Shendure J, Fields S, Blau CA, Noble WS. A three-dimensional model of the yeast genome. Nature. 2010; 465:363–367. [PubMed: 20436457]

Finan K, Cook PR, Marenduzzo D. Non-specific (entropic) forces as major determinants of the structure of mammalian chromosomes. Chromosome Res. 2011; 19:53–61. [PubMed: 20714801]

Gasser SM. Visualizing chromatin dynamics in interphase nuclei. Science. 2002; 296:1412–1416. [PubMed: 12029120]

Haase J, Stephens A, Verdaasdonk J, Yeh E, Bloom K. Bub1 kinase and Sgo1 modulate pericentric chromatin in response to altered microtubule dynamics. Curr Biol. 2012; 22:471–481. [PubMed: 22365852]

Haber JE, Leung WY. Lack of chromosome territoriality in yeast: promiscuous rejoining of broken chromosome ends. Proc Natl Acad Sci U S A. 1996; 93:13949–13954. [PubMed: 8943041]

Haering CH, Jessberger R. Cohesin in determining chromosome architecture. Exp Cell Res. 2012; 318:1386–1393. [PubMed: 22472347]

Hediger F, Neumann FR, Van Houwe G, Dubrana K, Gasser SM. Live imaging of telomeres: yKu and Sir proteins define redundant telomere-anchoring pathways in yeast. Curr Biol. 2002; 12:2076–2089. [PubMed: 12498682]

Heun P, Laroche T, Shimada K, Furrer P, Gasser SM. Chromosome dynamics in the yeast interphase nucleus. Science. 2001; 294:2181–2186. [PubMed: 11739961]

Hill A, Bloom K. Genetic manipulation of centromere function. Mol Cell Biol. 1987; 7:2397–2405. [PubMed: 3302676]

Hubner MR, Spector DL. Chromatin dynamics. Annu Rev Biophys. 2010; 39:471–489. [PubMed: 20462379]

Ira G, Hastings PJ. DNA breakage drives nuclear search. Nat Cell Biol. 2012; 14:448–450. [PubMed: 22552144]

Jendrejack RM. Stochastic simulations of DNA in flow: Dynamics and the effects of hydrodynamic interactions. J Chem Phys. 2002; 116:7752.

Jin QW, Fuchs J, Loidl J. Centromere clustering is a major determinant of yeast interphase nuclear organization. J Cell Sci. 2000; 113(Pt 11):1903–1912. [PubMed: 10806101]

Jones JJ, van der Maarel JR, Doyle PS. Effect of nanochannel geometry on DNA structure in the presence of macromolecular crowding agent. Nano Lett. 2011; 11:5047–5053. [PubMed: 21988280]

Kamiti M, van de Ven TGM. Measurement of spring constants of polyacrylamide chains bridging particles to a solid surface. Macromolecules. 1996; 29:1191–1194.

Levene, H. Robust tests for quality of variances.. In: Olkin, I., editor. Contribution to probability and statistics: essays in honour of Harold Hotelling. Stanford University Press; Stanford, NJ: 1960. p. 278-292.

Mine-Hattab J, Rothstein R. Increased chromosome mobility facilitates homology search during recombination. Nat Cell Biol. 2012; 14:510–517. [PubMed: 22484485]

Neumann FR, Dion V, Gehlen LR, Tsai-Pflugfelder M, Schmid R, Taddei A, Gasser SM. Targeted INO80 enhances subnuclear chromatin movement and ectopic homologous recombination. Genes Dev. 2012; 26:369–383. [PubMed: 22345518]

O'Toole ET, Winey M, McIntosh JR. High-voltage electron tomography of spindle pole bodies and early mitotic spindles in the yeast Saccharomyces cerevisiae. Mol Biol Cell. 1999; 10:2017–2031. [PubMed: 10359612]

Rabl C. Über Zelltheilung. Morph Jb. 1885; 10:214–330.

Rosa A, Everaers R. Structure and dynamics of interphase chromosomes. PLoS Comput Biol. 2008; 4:e1000153. [PubMed: 18725929]

Sanyal A, Bau D, Marti-Renom MA, Dekker J. Chromatin globules: a common motif of higher order chromosome structure? Curr Opin Cell Biol. 2011; 23:325–331. [PubMed: 21489772]

Scheffold F, Diaz-Leyva P, Reufer M, Ben Braham N, Lynch I, Harden JL. Brushlike Interactions between Thermoresponsive Microgel Particles. Physical Review Letters. 2010; 104

Schober H, Kalck V, Vega-Palas MA, Van Houwe G, Sage D, Unser M, Gartenberg MR, Gasser SM. Controlled exchange of chromosomal arms reveals principles driving telomere interactions in yeast. Genome Res. 2008; 18:261–271. [PubMed: 18096749]

Seitan VC, Merkenschlager M. Cohesin and chromatin organisation. Curr Opin Genet Dev. 2012; 22:93–100. [PubMed: 22155130]

Sofueva S, Hadjur S. Cohesin-mediated chromatin interactions--into the third dimension of gene regulation. Brief Funct Genomics. 2012; 11:205–216. [PubMed: 22278832]

Soutoglou E, Misteli T. Mobility and immobility of chromatin in transcription and genome stability. Curr Opin Genet Dev. 2007; 17:435–442. [PubMed: 17905579]

Spector DL. The dynamics of chromosome organization and gene regulation. Annu Rev Biochem. 2003; 72:573–608. [PubMed: 14527325]

Stephens AD, Haase J, Vicci L, Taylor RM 2nd, Bloom K. Cohesin, condensin, and the intramolecular centromere loop together generate the mitotic chromatin spring. J Cell Biol. 2011; 193:1167–1180. [PubMed: 21708976]

Stephens AD, Haggerty RA, Vasquez PA, Vicci L, Snider CE, Shi F, Quammen C, Mullins C, Haase J, Taylor RM 2nd, et al. Pericentric chromatin loops function as a nonlinear spring in mitotic force balance. J Cell Biol. 2013; 200:757–772. [PubMed: 23509068]

Taddei A, Gasser SM. Structure and function in the budding yeast nucleus. Genetics. 2012; 192:107–129. [PubMed: 22964839]

Taddei A, Schober H, Gasser SM. The budding yeast nucleus. Cold Spring Harb Perspect Biol. 2010; 2:a000612. [PubMed: 20554704]

Tjong H, Gong K, Chen L, Alber F. Physical tethering and volume exclusion determine higher-order genome organization in budding yeast. Genome Res. 2012; 22:1295–1305. [PubMed: 22619363]

Tokuda N, Terada TP, Sasai M. Dynamical modeling of three-dimensional genome organization in interphase budding yeast. Biophys J. 2012; 102:296–304. [PubMed: 22339866]

Uhlenbeck GE, Ornstein LS. On the Theory of the Brownian Motion. Phys Rev. 1930; 36:823–841.

Verdaasdonk JS, Gardner R, Stephens AD, Yeh E, Bloom K. Tension-dependent nucleosome remodeling at the pericentromere in yeast. Mol Biol Cell. 2012; 23:2560–2570. [PubMed: 22593210]

Wan, X. Dept. of Biomedical Engineering. University of North Carolina at Chapel Hill; Chapel Hill, N.C.: 2008. Asymmetric chromosome oscillation during mitosis and protein architecture of the human kinetochore measured by K-SHREC Kinetochore-Speckle High Resolution Co-Localization.; p. 1electronic text PDF (2.63 MB)

Wan X, Cimini D, Cameron LA, Salmon ED. The coupling between sister kinetochore directional instability and oscillations in centromere stretch in metaphase PtK1 cells. Mol Biol Cell. 2012; 23:1035–1046. [PubMed: 22298429]

Wan X, O'Quinn RP, Pierce HL, Joglekar AP, Gall WE, DeLuca JG, Carroll CW, Liu ST, Yen TJ, McEwen BF, et al. Protein architecture of the human kinetochore microtubule attachment site. Cell. 2009; 137:672–684. [PubMed: 19450515]

Weber SC, Spakowitz AJ, Theriot JA. Nonthermal ATP-dependent fluctuations contribute to the in vivo motion of chromosomal loci. Proc Natl Acad Sci U S A. 2012; 109:7338–7343. [PubMed: 22517744]

Wong H, Marie-Nelly H, Herbert S, Carrivain P, Blanc H, Koszul R, Fabre E, Zimmer C. A predictive computational model of the dynamic 3D interphase yeast nucleus. Curr Biol. 2012; 22:1881–1890. [PubMed: 22940469]

Zimmer C, Fabre E. Principles of chromosomal organization: lessons from yeast. J Cell Biol. 2011; 192:723–733. [PubMed: 21383075]

Highlights

- Chromatin tethering at the centromere and telomere affect confinement and stiffness

- Cohesin depletion results in reduced confinement and effective spring constant

- Nucleosome depletion leads to increased confinement and effective spring constant

- Tethering and confinement underlie chromosome territory formation and fluctuation
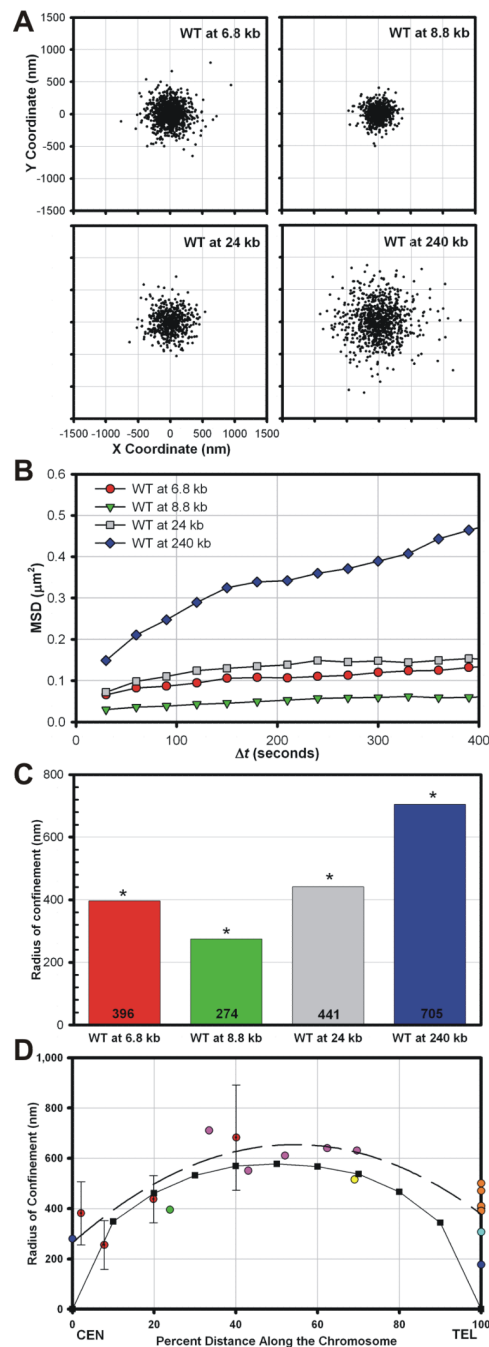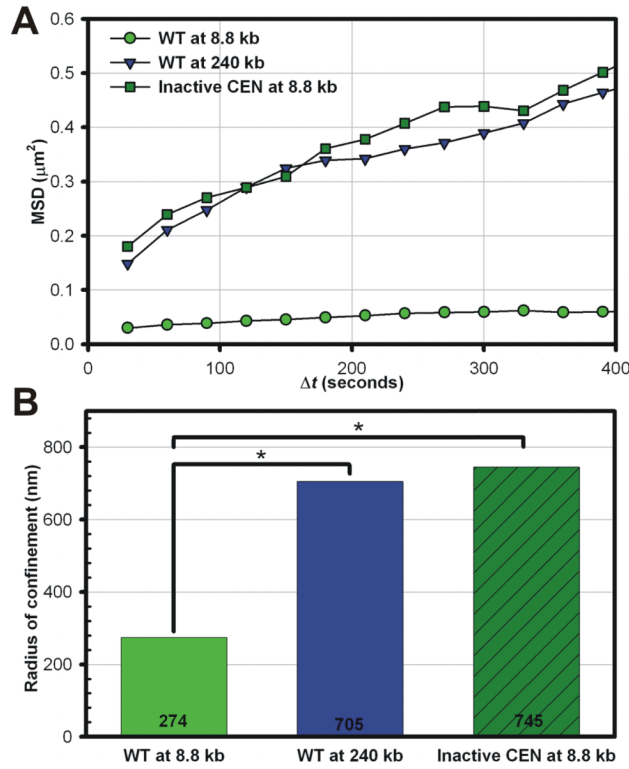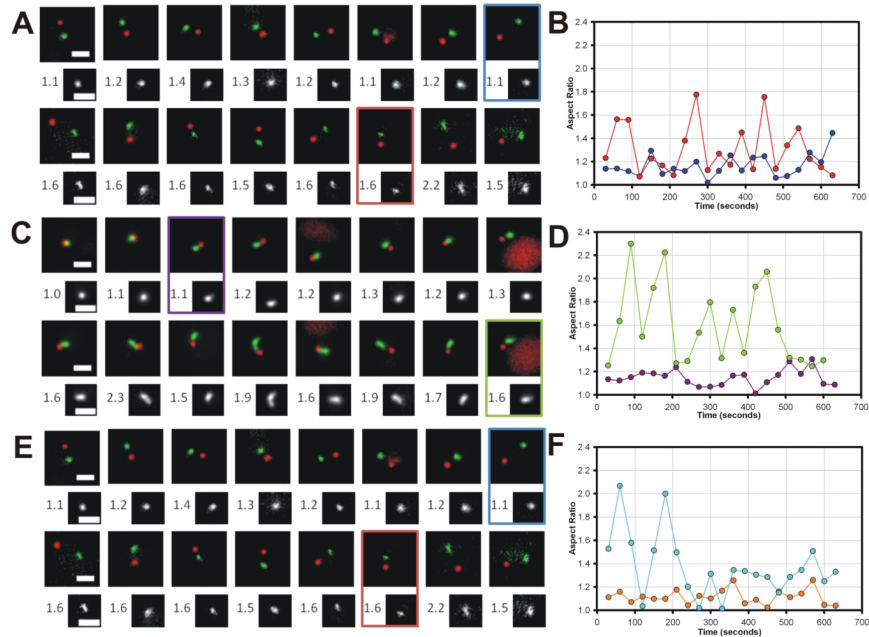
Figure 1.
R_c of chromatin varies along the length of the chromosome. **(A)** Scatter plots illustrating variance in WT lacO/lacI-GFP spot position relative to spindle pole body. **(B)** MSD curves of WT chromatin spot motion at various distances from the centromere. **(C)** R_c values calculated using Equation 2 and whole population standard deviation values (Table 1). R_c values are all significantly different from each other (Levene's test, p<0.05, Figure S2A). For comparison of R_c calculations using Equations 1 and 2, see Table S1 and Figure S1A. **(D)** Experimental and literature R_c values plotted by percent distance from centromere (0%) and telomere (100%). The dashed line illustrates the general trend of reduced confinement at

increasing distances from the attachment point. Red – this work using individual cell variance, mean ± standard deviation (Table S1); orange – (Bystricky et al., 2005); yellow – (Dion et al., 2012); light blue – (Hediger et al., 2002); dark blue – (Heun et al., 2001); green – (Mine-Hattab and Rothstein, 2012); purple – (Neumann et al., 2012); black squares – our tethered bead-spring model (see text).
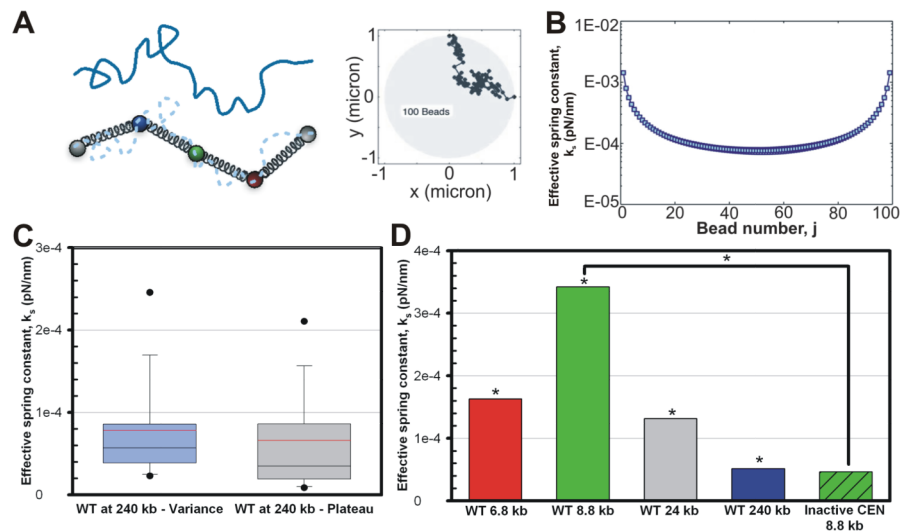
Figure 2.
R_c is dictated by the attachment at the centromere. **(A)** MSD analysis of cells in which the centromere has been detached through its conditional inactivation (Gal-CEN on GAL) revealed reduced confinement of a lacO/lacI-GFP labeled chromatin spot 8.8 kb from the CEN as compared to WT at 8.8 kb. **(B)** Bar graph of R_c values (Equation 2). Statistical comparison show WT at 8.8 kb and Inactive CEN at 8.8 kb to be statistically significantly different from each other, whereas WT at 240 kb and Inactive CEN at 8.8 kb are not statistically significantly different from each other (Levene's test, $p<0.05$, Figure S2A).
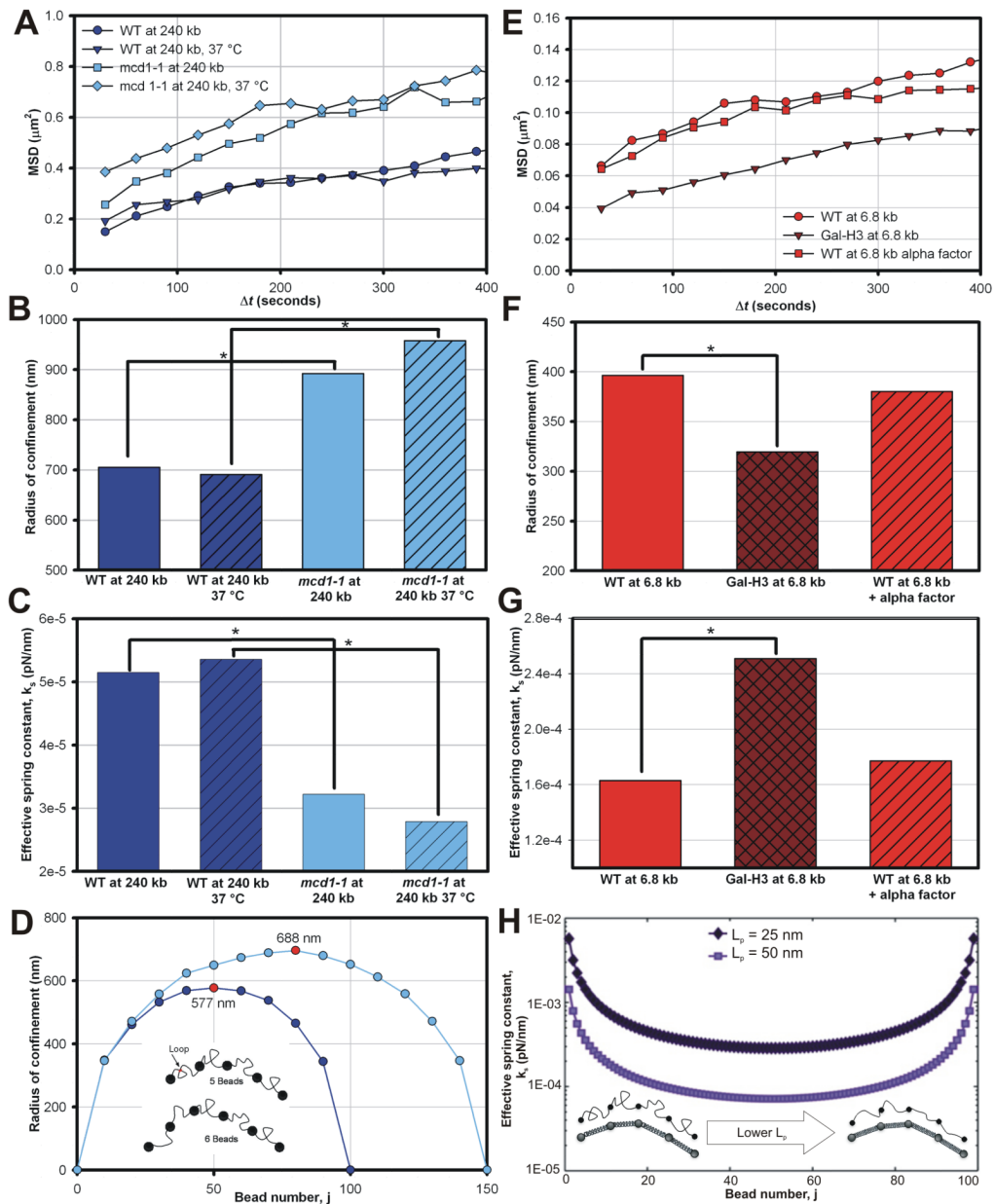
Figure 3.
Interphase chromatin is dynamic. (**A**) Example images of lacO/lacI-GFP at 240 kb from the CEN with aspect ratios less than and greater than 1.5 (compacted and decompacted). Measured aspect ratios are shown. (**B**) Graph of aspect ratio change over time for two cells, colors corresponding to outlined images in (A). (**C**) Example images of lacO/lacI-GFP at 6.8 kb and (**D**) graphs of aspect ratio changes for two examples. WT cells exhibit transient expansion and recompaction of chromatin arrays along random and occasionally non-linear trajectories. (**E**) Example images of lacO/lacI-GFP at 6.8 kb in Gal-H3 cells in which nucleosomes have been depleted (see text), and (**F**) graphs of aspect ratio changes over time. Aspect ratio values of lacO/lacI-GFP signal =large axis/small axis. Scale bar = 1 μm. Time lapse images were taken every 30 s. Color images: lacO/lacI-GFP – green, and spindle pole body (Spc29-RFP) – red. Black and white images show lacO/lacI-GFP with corresponding aspect ratios alongside.

Figure 4.
Modeling interphase chromatin dynamics as a doubly tethered bead-spring polymer chain. **(A)** The chromatin polymer (dark blue) can be modeled as a bead-spring polymer chain (dotted blue line indicates original chromatin polymer chain). Diagram of a bead-spring chain composed of 100 beads tethered at both ends and confined within a circle of radius 1 μm. **(B)** The effective spring constant (k_s, Equation 3) is highest (most stiff) for beads closest to the tether points (beads 0 and 100) and softest in the middle of the chain (at bead 50). **(C)** Measurement of k_s from *in vivo* dynamic MSD data at various positions from the centromere. We compared k_s calculated using the MSD plateau value (gray, Equation 4) or the variance of the distribution of spot positions (light blue, Equation 5) and found no significant difference in WT cells at 240 kb from the CEN (Student's t-test, $p > 0.05$, Table S1). Black bars indicate median, red bars indicate mean. Black dots above and below indicate 95%/5% percentiles of the data distribution. (For comparisons at 24 kb, 8.8 kb, and 6.8 kb from the CEN, see Figure S1B). **(D)** K_s values calculated using the variance of the distribution of spot positions of the whole population (Equation 5, Table 1). Consistent with the doubly tethered bead-spring polymer chain model, the chromatin exhibited a higher k_s (stiffer spring) closer to the tether point (at 6.8 kb and 8.8 kb from the CEN), and lower k_s (softer spring) in the middle of the chromosome (at 240 kb from the CEN). The high k_s observed close to the centromere is due to attachment at the centromere and is not an inherent property of this region of chromatin. When the centromere is detached through its conditional inactivation (Inactive CEN), the k_s at 8.8 kb from the CEN is reduced. Statistical comparisons at four WT positions are statistically significantly different from each other. Upon conditional centromere inactivation (Inactive CEN), the measured k_s at 8.8 kb is significantly softer from the measured k_s for WT at 8.8 kb (Levene's test, $p < 0.05$, Figure S2A).
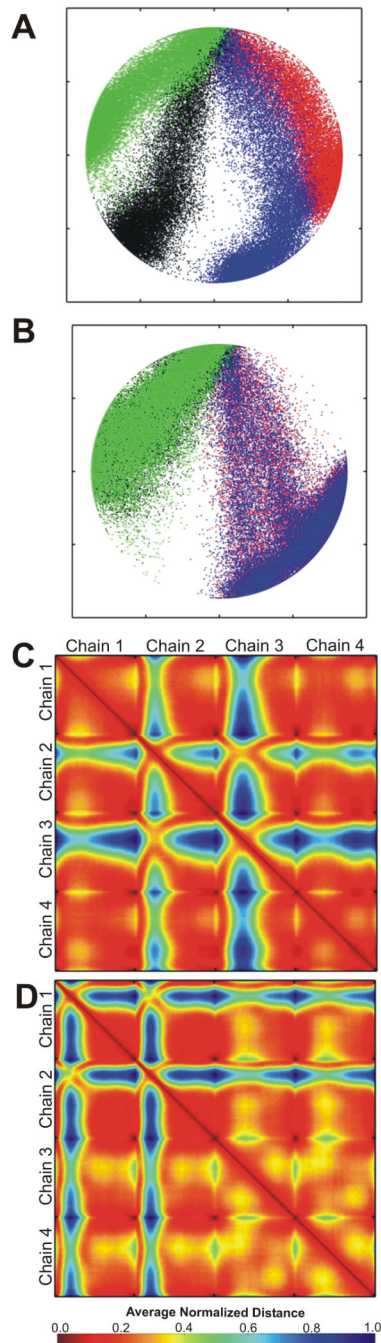
Figure 5.
Loss of cohesin or nucleosome depletion during interphase result in altered confinement and chromatin stiffness. **(A)** Upon depletion of cohesin (*mcd1-1* at 37 °C, light blue diamonds) we observed a decrease in confinement of chromatin at 240 kb from the CEN that is not due to the increased temperature (compare to WT at 37 °C, dark blue triangles). **(B)** Bar graph of R_c values (Equation 2). Statistical comparisons reveal significant increased R_c upon depletion of cohesin in *mcd1-1* cells (Levene's test, p<0.05, Figure S2B). **(C)** K_s (Equation 5) is reduced (softened) upon depletion of cohesin as compared to WT at 24 °C and 37 °C. **(D)** We can simulate the effects of depleting cohesin and losing chromatin looping as an increase in the number of beads in our model (inset). This predicts that increasing the number of beads in the chain will result in reduced confinement (688 nm) as compared to the same bead position (middle, red circle) on a shorter chain (577 nm), consistent with experimentally observed data. **(E)** MSD curves of lacO/lacI-GFP at 6.8 kb from the CEN in

WT, histone depleted (Gal-H3) and α factor treated cells. **(F)** R_c is reduced (more confined, Equation 2) and **(G)** effective k_s is increased (stiffer, Equation 5) upon depletion of histone H3. Statistical comparisons show a significant difference in both R_c and k_s upon histone depletion ($p < 0.05$) and no significant difference upon α factor treatment ($p > 0.05$) (Levene's test, $p < 0.05$, Figure S2C). **(H)** We hypothesize that reducing nucleosome density by depleting histone H3 will result in reduced L_p (from chromatin to DNA, (Bloom, 2008)). Our doubly tethered bead-spring model predicts an increase in k_s upon reduction of L_p (from $L_p = 50$ to $L_p = 25$ nm), consistent with experimentally observed increase in k_s at 6.8 kb from the CEN upon nucleosome depletion.

Figure 6.
Modeling the chromatin spring as a doubly tethered, confined bead-spring chain with excluded volume interactions can recapitulate chromosome territory formation as observed by chromosome interaction heat maps. We have tracked bead positions over time for a single run for chains in which one end (centromere-SPB attachment) is at the top of the circle (at 0 degrees) and the other end (telomere attachment) is tethered at **(A)** four discrete positions (equally distributed between 90 and 298 degrees) or **(B)** tethered at two discrete positions (90 and 298 degrees). Heat map representation for the average distance during a run between all beads for **(C)** four discrete attachment points and **(D)** two attachment points. Heat map values have been normalized to 1 to account for different maximum distances

between model runs. For a value of 0, the beads are separated by a small distance and thus highly likely to come into physical contact, whereas a value of 1 represents a large spatial separation and low probability of contact. Chain 1 – red; chain 2 – blue; chain 3 – black; chain 4 – green.

TABLE 1

Summary of R_c and k_s measurements from population variance

LacO array distance from centromere	Relevant genotype/conditions	Sample size	Radius of confinement (R_c) (nm) $= \frac{5}{4} * \sqrt{2\sigma^2 + \langle \Delta r_0^2 \rangle}$ (population σ)	Effective spring constant (ks) (pN/nm) $= \frac{k_B T}{\sigma^2}$ (population σ)	Fold over entropic spring
240 kb	WT (Chr II)	43	705	5.1×10^{-5}	33×
24 kb	WT (Chr III)	25	441	1.3×10^{-4}	9×
8.8 kb	WT (Chr III)	40	274	3.4×10^{-4}	8×
6.8 kb	WT (Chr XV)	54	396	1.6×10^{-4}	3×
8.8 kb	Gal-CEN on galactose	23	745	4.6×10^{-5}	1×
240 kb	WT, 37C	16	691	5.4×10^{-5}	35×
240 kb	*mcd1-1*	25	892	3.2×10^{-5}	21×
240 kb	*mcd1-1*, 37C	33	958	2.8×10^{-5}	18×
6.8 kb	Gal-H3 on glucose	55	319	2.5×10^{-4}	5×
6.8 kb	WT, α factor	43	380	1.8×10^{-4}	3×